THE ROPER RESONANCE AND KIN

Volker Burkert [a], Eberhard Klempt [b,a]

[a]Thomas Jefferson National Accelerator Facility, Newport News, VA, USA
[b]Helmholtz-Institute für Strahlen- und Kernphysik
der Rheinischen Friedrich-Wilhelms Universität
Nussallee 14–16, 53115 Bonn, Germany

Received 24 October 2025, accepted 3 November 2025,
published online 10 February 2026

The properties of the Roper resonance $N(1440)1/2^+$ are reviewed. Quark models have long struggled to reproduce its mass relative to its negative-parity partner $N(1535)1/2^-$. This discrepancy motivated interpretations of the Roper as a dynamically generated meson–baryon state. Including its isospin partners $\Delta(1600)3/2^+$ and $\Delta(1700)3/2^-$ further accentuates the tension between quark-model predictions and experiment. Recent developments based on AdS/QCD and functional methods achieve much improved agreement, identifying the Roper as an ordinary three-quark excitation. Electroproduction experiments at Jefferson Lab have now resolved this long-standing question, revealing the Roper as a qqq core dressed by a substantial meson cloud. The Roper resonance belongs to a family of four N^* states with $J^P = 1/2^+$; the highest-mass member, $N(2100)1/2^+$, likely represents a Roper-like excitation in the fourth shell.

DOI:10.5506/APhysPolB.57.2-A4

1. Introduction

The Roper resonance — what a name for a particle! It is the only known resonance named after its discoverer. Why is it important? The resonance is frequently and extensively discussed in the literature, yet it is comparatively rarely cited: 189 articles include the name "Roper" in their title, but only 40 of them cite David's original paper[1]. "The Roper" seems to have become as established a term as "the proton". In both cases, there appears to be no need to cite the discoverer. But what makes $N(1440)1/2^+$ so special?

[1] As of October 16, 2025.

In 1964, when David published his celebrated paper [1], baryon spectroscopy was still in its infancy. More than a decade earlier, Enrico Fermi had used a π^+ meson beam scattering off protons in a hydrogen target [2]. The cross section showed a sharp rise from the pion-production threshold up to about 1200 MeV — a strong indication of the first baryon resonance, now known as $\Delta(1232)3/2^+$. The pion beam energy at that time, however, was insufficient to reveal the full resonance profile.

In the following years, a few other resonances were discovered. Each appeared as a distinct peak in the cross section and exhibited characteristic features in the observables that revealed their spin and parity. David's resonance was different. He wrote: "The resonance suggested in this paper, however, is not associated with conspicuous features in the observables measured so far and has been inferred from a more quantitative analysis". David's work marked the beginning of a new era: the identification of resonances not through visible peaks, but through quantitative analyses. It became clear that resonances should not be defined merely by peaks in invariant mass spectra, but rather by studying the analytic behavior of complex scattering amplitudes.

The original motivation for David's study of πN interactions was to confirm a P_{11} structure observed by Feld and Layson at a mass of about 1690 MeV in the ΛK invariant mass [3]. These authors found that the ΛK peak was compatible with πN scattering amplitudes. The ΛK structure may well correspond to what we now identify as $N(1710)1/2^+$.

Later, David's surprising result — that the P_{11} wave of the πN scattering amplitude resonates at a mass as low as 1440 MeV — posed a serious challenge to the theoretical models that were subsequently developed. The low mass could not be easily explained within quark models and sparked a long-standing debate about its nature, see also [4].

At the heart of this debate lies a fundamental question: What is a resonance? Formally, we define resonances as poles in the complex scattering plane. But what physical mechanisms give rise to them? Are they generated by internal quark dynamics? Are all resonances of this kind? Or are some driven by molecular-type meson–baryon forces — perhaps all of them? Could every resonance be understood as a hadronic molecule?

2. Properties of the Roper resonance

The Roper resonance, or $N(1440)1/2^+$ as it is known today, has been studied in numerous experiments, often yielding partly inconsistent results. Figure 1 shows the distribution of measured masses as reported in the Review of Particle Physics (RPP) [5]. Each entry is represented by a box whose width corresponds to the quoted uncertainty and whose height is proportional to the inverse of that uncertainty.

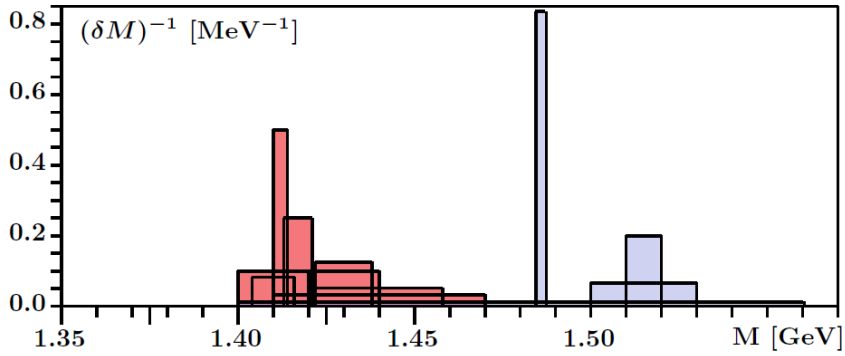

Fig. 1. Breit–Wigner masses from all entries in the RPP [5]. The box widths give the uncertainty, the height is inversely proportional to the uncertainty. The data are from Refs. [6–14] (low mass) and [14–16] (high mass). See the text for a discussion.

The measurements cluster into two distinct groups: a high-mass cluster, primarily originating from data published before 2010, and a low-mass cluster, reported mostly after that year. Only Höhler [6, 17] and Cutkosky [7] had already reported low Roper masses at an early stage.

In determining the properties of the Roper resonance, results from publications reporting high Roper masses are excluded. However, all results listed in the RPP are included here, regardless of whether they were used in the averaging procedure.

Tables 1 and 2 summarize the properties defined at the pole and in Breit–Wigner (BW) parameterizations: pole positions, helicity amplitudes at the pole, BW masses and widths, and BW helicity amplitudes.
The reported values, *e.g.* for the pole mass, are statistically inconsistent. Most publications quote only statistical uncertainties, while systematic shifts in the mass can arise from various sources: amplitudes that do not fully satisfy theoretical constraints such as unitarity, analyticity, or crossing symmetry; incomplete inclusion or insufficient experimental constraints on allowed decay modes; or limitations in the model space, such as the number of resonances included across partial waves. These factors can all have a significant impact on the extracted results. We therefore estimate the overall uncertainty from the statistical spread of the published values.

The penultimate line lists the range of values defined by the PDG, while the final line gives the mean value and its associated uncertainty.

Most observables are consistently described with reasonably small uncertainties, with the notable exception of the $N(1440)1/2^+ \to N\rho$ branching ratio. This quantity depends critically on the precise definition of the ratio [18].

Table 1. Properties of the Roper resonance at the pole: mass, widths, the elastic pole residue $r \exp i\vartheta$ (r in MeV, ϑ in degree), and helicity amplitudes (in 10^{-3} GeV$^{-1/2}$). The last two rows give the ranges suggested by the Particle Data Group and our mean values and their uncertainties.

$M_{\rm pole}$	$\Gamma_{\rm pole}$	$\lvert r\rvert$	ϑ	$A^{\rm pole}_{1/2}$	phase	Ref.
1366±3	192±4			−60±6	−(30±7)°	[12]
1374±5	215±20	58±23	−(65±11)°			[19]
1353±1	203±2	59±1	−(104±2)°	−90±7	−(30±3)°	[20]
1360	186	49±3				[11]
1370±4	190±7			*41±5*	*(23±10)*°	[21]
1369±3	189±5	49±3	−(82±3)°	−44±5	−(40±8)°	[10]
1355	215	62	−98°	−60	−23°	[22]
1363±3	180±6	50±2	−(88±2)°			[23]
1375±30	180±40	52±5	−(100±35)°			[7]
1385	164	40				[6, 17]
1360–1380	180–205	50–60				[5]
1367±10	191±16	52±7	−(90±15)°	−65±19	−(33±9)°	mean

Table 2. Breit–Wigner properties of the Roper resonance: masses, widths (in MeV), helicity amplitudes $N(1440)1/2^+ \to p\gamma$ (in 10^{-3} GeV$^{-1/2}$), and branching ratios. The decay into $N\rho$ can proceed with angular momentum $l = 0$ and ρ and nucleon spins add to $S = 1/2$, or with $l = 2, S = 3/2$. Helicity amplitudes for $N(1440)1/2^+ \to n\gamma$ are given in italic.

$M_{\rm BW}$	$\Gamma_{\rm BW}$	$A^{\rm BW}_{1/2}$	$N\pi$	$\Delta\pi$	$N\rho_0$	$N\rho_2$	$Nf_0(500)$	Ref.
1410±10	290±30	−76±8		15±7	9±4	9±4	15±5	[12]
1417±4	257±11	−91±7	59±2	22±4	1.3±0.4		16±3	[11]
1430±10	360±30	−61±6	63±2	20±7			15±6	[10]
1412±2	248±5	−84±3	85±1	7±1	1.3±0.4		27±1	[9]
1439±19	437±151		62±4					[8]
1440±30	340±70		68±4					[7]
1410±12	135±10		51±5					[6]
1410–1470	250–450	−80 to −50	55–75					[5]
1423±13	295±96	−78±13	65±10	16±7			18±7	mean

$A^{\rm BW}_{1/2\ N(1440)\to p\gamma}$	*13±12* [11]	*53±7* [21]	*48±4* [24]	*35 to 55* [5]	*38±22*	mean

The partial decay width for the S-wave decay is given by

$$\Gamma_0(s) = \frac{g_0^2}{\sqrt{s_0}}\,\rho_0(s), \tag{1}$$

where s (s_0) is the squared invariant mass (at the resonance mass), $\rho(s) = 2p/(16\pi\sqrt{s})$ is the two-body phase space with p the decay momentum, and g_0 is a a coupling constant. For the D-wave decay, this term is multiplied by a centrifugal barrier factor. Conventionally, the branching ratio is defined at the nominal mass of the resonance, with $\mathrm{BR}_0 = \Gamma_0(s_0)/\Gamma_{\mathrm{tot}}$, and the partial width $\Gamma_0(s_0) = 0$ due to the vanishing phase space.

However, the high-mass tail of the $N(1440)1/2^+$ resonance can decay into $N\rho$, particularly into the low-mass tail of ρ mesons. This effect can be properly accounted for by integrating Eq. (1) over the mass distributions of both the parent and daughter resonances.

3. Interpretations of the Roper resonance

The Roper resonance is the lowest-mass state with the quantum numbers of the nucleon. Only a few years after its discovery, it had already become the subject of considerable controversy. In Ref. [25], the Roper resonance was interpreted as primarily an $Nf_0(500)$ [2] self-consistent bound state, consistent with the bootstrap picture of hadron resonances. In Ref. [26], $N(1440)1/2^+$ was instead proposed to be the first radial excitation of the nucleon.

Since then, these two competing interpretations — whether the Roper resonance is a dynamically generated state or an ordinary three-quark excitation — have accompanied its study and shaped the ongoing discussion of its nature [27].

In the first consistent quark-model calculation of the baryon resonance spectrum, Isgur and Karl assumed a linear confining potential, combined with an effective one-gluon exchange [28, 29]. A large number of alternative models were subsequently developed. One serious problem soon emerged: as a three-quark state, the Roper resonance — belonging to the second excitation shell — appeared with a lower mass than $N(1535)1/2^-$, which belongs to the first excitation shell. This inversion is difficult to explain.

In Fig. 2, the experimental masses of the Roper resonance and its nearby negative-parity partner, $N(1535)1/2^-$, are compared with theoretical predictions. Model parameters are often tuned to reproduce the experimental values; therefore, we also compare the corresponding pair of resonances in the Δ sector: $\Delta(1600)3/2^+$, the first radial excitation of $\Delta(1232)3/2^+$, and $\Delta(1700)3/2^-$, the first orbital excitation with $J = 3/2$.

[2] Referred to as S_0 with a mass of 700 MeV.

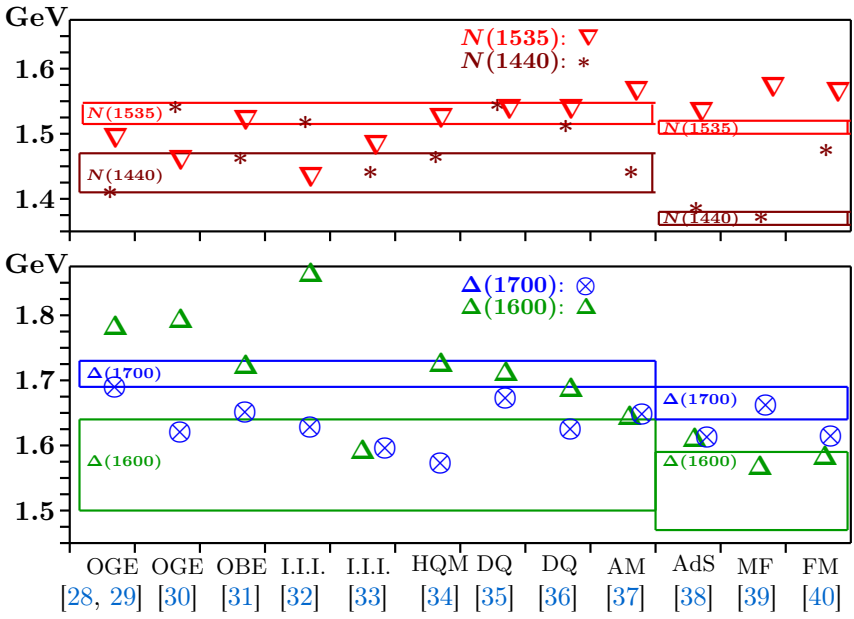

Fig. 2. Comparison of calculated masses of spin-1/2 nucleon and spin-3/2 Δ resonances with RPP values (shown by boxes). The models are characterized by their interaction: One-gluon exchange (OGE) [30], Goldstone-boson exchange (GBE) [31], instanton-induced interactions (I.I.I.) without [32] or with additional Goldstone-boson exchange [33], the hypercentral constituent-quark model (HQM) [34], diquark (DQ) models [35, 36], the algebraic model (AM) [37], a holographic model [38], an empirical mass formula (MF) [39], and functional methods (FM) [40]. The three latter models are compared to the pole masses.

In most dynamical models, the mass ordering $M_{N(1440)1/2^+} > M_{N(1535)1/2^-}$ is obtained, contrary to experiment. In those cases where the ordering is correct, $M_{\Delta(1600)3/2^+} > M_{\Delta(1700)3/2^-}$, the predicted $\Delta(1600)3/2^+$ mass is usually considerably too high. Reasonable agreement with the data is achieved only in Refs. [37, 39] and [38, 40]. The latter two are QCD-based approaches starting from quarks with (nearly) vanishing current masses.

These two QCD-based models are conceptually very different. Reference [38] employs light-front holographic QCD, exploiting the correspondence between gravity in anti-de Sitter (AdS) space and a conformal field theory. Reference [40], by contrast, uses functional methods derived from the path integral formalism, converting classical equations of motion (Klein–Gordon, Dirac, and Maxwell equations) into their quantum counterparts such as the Dyson–Schwinger equations. Both approaches are firmly grounded in QCD. Their results demonstrate that the low mass of the Roper resonance should no longer be regarded as an unresolved problem.

The difficulties of early models in reproducing the low masses of the Roper and $\Delta(1600)3/2^+$ resonances led to interpretations of $N(1440)1/2^+$ beyond the traditional quark model. In the bag model, the Roper may represent a collective vibration of the bag surface. Indeed, within the Skyrme model — where baryons appear as topological solitons of non-linear meson fields — a resonance was found in the breathing mode at $M = 1420$ MeV [41]. Alternatively, the Roper could have a large gluonic component [42], denoted $qqqg$. Such "hybrid" states were two decades later predicted by the lattice QCD, although at significantly higher masses [43].

The authors of [44] investigated the Roper resonance within a coupled-channel meson-exchange model including $\Delta(1232)\pi$, $N\rho$, and $Nf_0(500)$ channels. They found that the Roper resonance can be described purely by meson–baryon dynamics — without the need to introduce an explicit three-quark core — to reproduce πN phase shifts and inelasticities. The resonance thus emerges dynamically. These results were confirmed in Refs. [45, 46], where both $N(1440)1/2^+$ and $\Delta(1600)3/2^+$ were dynamically generated without requiring genuine three-quark components. Similarly, Ref. [47] identifies the Roper as a dynamically generated state with negligible contributions from bare states, while Ref. [48] finds that the dominant contributions to $\Delta(1600)3/2^+$ arise from strong rescattering in the πN and $\pi\Delta(1232)$ channels, interpreting $\Delta(1600)3/2^+$ as a dynamically generated resonance.

The internal structure of the Roper resonance — whether it is a three-quark state, a hybrid, or a meson–baryon molecule — cannot be inferred from its mass alone. Its true nature can only be determined through electroproduction experiments spanning a wide range of momentum transfers.

4. Electroproduction of the Roper resonance

We first briefly discuss how meson electroproduction contributes to elucidating the nature of the excited states. The virtual (spacelike) photon exchanged between the scattered electron and the target nucleon has a finite lifetime and, correspondingly, probes the nucleon's interior within a limited spatial domain. The higher the photon virtuality Q^2, the shorter its lifetime, and the finer the spatial resolution that can be achieved.

Excitation of the ground-state nucleon through electron scattering in the s-channel provides a powerful means of investigating the structural properties of the excited states. The Roper resonance, as the lowest-mass nucleon resonance, exhibits many features — such as structural complexity — comparable to those of higher-mass resonances, and may thus serve as a representative example of the latter.

In the following, we employ the Q^2-dependence of the excitation strength as a tool to disentangle the various contributions to the resonance strength and to identify the respective roles of the quark core and meson–baryon components. The Roper resonance, as a state with spin-parity $J^P = 1/2^+$ and isospin 1/2, can be studied most effectively on a proton target in the $ep \to e'\pi^+ n$ reaction. The kinematics for single π^+ production are shown in Fig. 3. The unpolarized differential cross section has four terms, or five

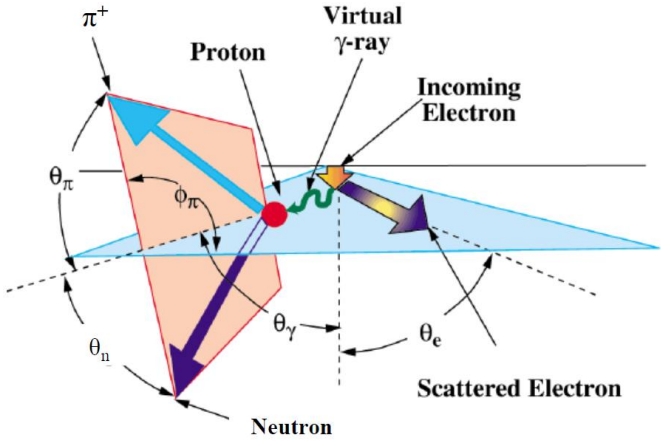

Fig. 3. Kinematics of π^+ electroproduction off protons in the laboratory system.

if the beam electrons are spin polarized. These terms relate to the transverse photon absorption cross section $\sigma_{\rm T}$, the longitudinal photon absorption cross section $\sigma_{\rm L}$, and the transverse–transverse interference terms $\sigma_{\rm TT}$, and transverse–longitudinal term $\sigma_{\rm TL}$. Measurement of all these cross sections in large acceptance detectors such as the CLAS at Jefferson Lab enables a detailed breakdown of the different electromagnetic contributions into the various partial wave elements underlying the production process. In the case of Roper-like resonances, the magnetic M_{1-} and the scalar S_{1-} are the relevant contributions leading to real and imaginary parts of the amplitude. The magnetic transition amplitude M_{1-} is shown in Fig. 4 for two values of $Q^2 = 0$ and $Q^2 = 2$ GeV^2, and as a function of the invariant mass $W = M(n\pi^+)$.

It shows that the resonance character of the Roper $N(1440)1/2^+$ is more prominently visible at high Q^2 in both the real and imaginary parts of the amplitude in comparison with the situation at $Q^2 = 0$. The resonance position is clearly seen in the peak of the imaginary parts M_{1-} at both values of Q^2. However, at $Q^2 = 0$, the real part clearly shows stronger and more extended contributions, which are not seen at the higher Q^2 value. This indicates the effects of more complex and extended contributions of

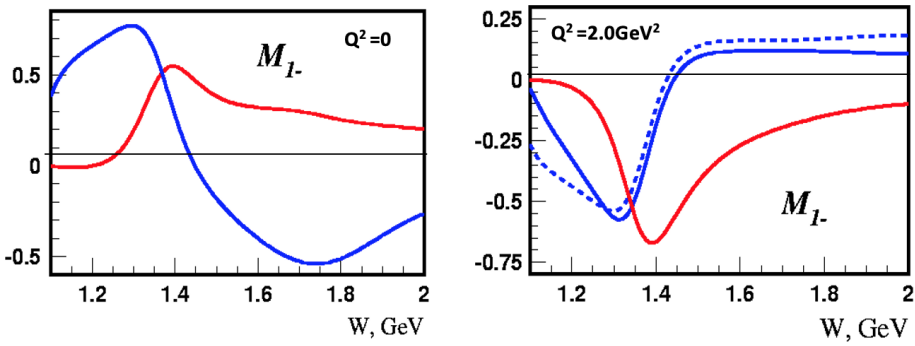

Fig. 4. Magnetic transition multipole M_{1-} of the proton to Roper resonance transition *versus* W. The red lines represent the imaginary part of M_{1-}, the blue lines the real part, using two different analysis techniques; left: $Q^2 = 0$, right: $Q^2 = 2$ GeV^2.

meson–baryon both in the imaginary, but especially in the real part of the M_{1-}, while at high Q^2, the coupling is consistent with a well-localized and spatially compact three-quark core.

Although the partial-wave analysis clearly shows the sign change and the strong excitation of the Roper resonance at the real-photon point and at high Q^2, a separation of the resonant and non-resonant contributions is required in order to compare the data with theoretical predictions and advanced quark-based models that do not include meson–baryon effects. The procedure used to separate the resonant parts of the magnetic and scalar transition multipoles M_{1-} and S_{1-} and to relate them to the amplitudes $A_{1/2}$ and $S_{1/2}$ is described in detail in [49, 50].

In Fig. 5, $A_{1/2}$ and $S_{1/2}$ are displayed as functions of Q^2, where $A_{1/2}$ represents the transition strength of the transverse virtual photon and $S_{1/2}$ that of the scalar (or longitudinal) virtual photon. Applying the Siegert theorem [51] in the long-wavelength limit leads to the constraint $S_{1/2} = 0$ at $\vec{Q}^2 = 0$, corresponding to the time-like region ($Q^2 < 0$). This partly explains the steep drop of the $S_{1/2}$ amplitude near the real-photon point.

The Q^2 dependence of the $A_{1/2}$ amplitude is particularly interesting. It starts at a large negative value near the real-photon point ($Q^2 = 0$) and rises steeply with increasing Q^2, changing sign near $Q^2 \approx 0.5$ GeV^2. A sign change in a transition amplitude (or transition form factor) is often associated with a node in the corresponding radial wave function and can therefore be interpreted as a first indication of the radial structure of the Roper resonance. We also note that this sign change in the $A_{1/2}$ amplitude is predicted by both theoretical approaches considered — the Dyson–Schwinger equation (DSE) framework and the light-front relativistic quark model (LF

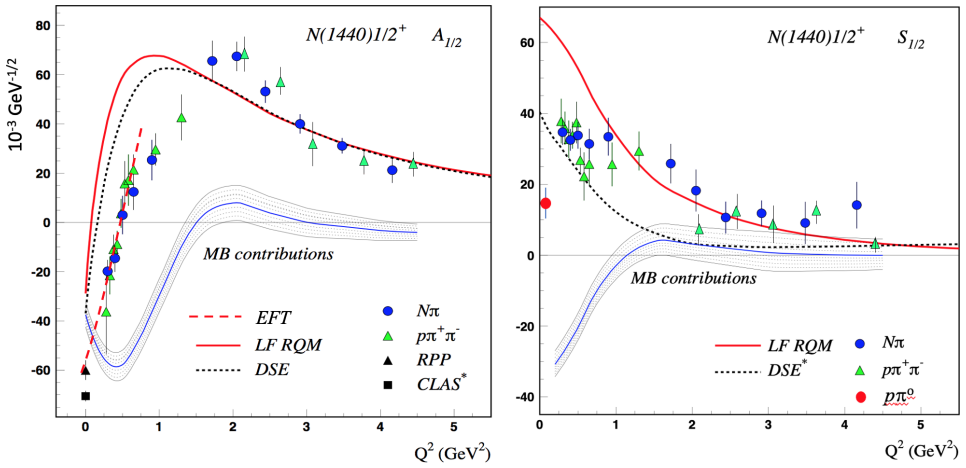

Fig. 5. Left: The $\gamma^* p \to N(1440)$ helicity transition amplitude $A_{1/2}$. Right: $S_{1/2}$. Both amplitudes are in units of 10^{-3} GeV$^{-1/2}$. The solid red curves are from a light-front relativistic quark model [52] and the black dashed curves are DSE results [53]. The green triangles and the blue full circle markers are data from the CLAS Collaboration [49, 54, 55]. The red circle at the very small Q^2 value is from [56]. See also the text for details.

RQM). Both calculations are based on the underlying quark structure of the resonance and are expected to reproduce the region $Q^2 > 1$–2 GeV^2, while the low-Q^2 domain, where meson–baryon contributions are significant, can only be described qualitatively within such models.

This is indeed observed: in both theoretical approaches, the node occurs at smaller values of Q^2 than in the data. This discrepancy is not unexpected, as the strong meson–baryon components in the Roper's wave function at low Q^2, which are not included in these models, are likely to affect the dynamics of the resonance transition.

Following the sign change, the transverse amplitude reaches a maximum positive value near $Q^2 \approx 1.5$ GeV^2, before gradually decreasing at higher Q^2. In this kinematic region, good agreement is observed between both theoretical predictions and the data. The meson–baryon contributions diminish rapidly above $Q^2 > 2$ GeV^2, as indicated by the shaded areas in Fig. 5.

For the scalar (longitudinal) transition amplitude $S_{1/2}$, a different and simpler trend is seen. Except for the very small Q^2 range discussed above, the amplitude decreases smoothly with increasing Q^2 and agrees with the LF RQM predictions for $Q^2 > 1.5$ GeV^2, consistent with the behavior of $A_{1/2}$. In contrast, the DSE approach predicts a significantly steeper falloff with Q^2 than is observed in the data.

4.1. Comparison of the Roper $N(1440)1/2^+$ with $N(1535)1/2^-$

The $N(1535)1/2^-$ resonance in the quark model is the first orbital excitation of the proton with one of the three quarks in an orbital state with $L_q = 1$ and negative parity. In the quark model, this state is thus the parity partner to the nucleon. Furthermore, similar to the Roper resonance, it is also considered a dominantly dynamically generated resonance [57] or as a meson–baryon molecule [58, 59]. Fortunately, there are data available at Jefferson Lab, both from CLAS in Hall B and from Hall C, that extend over the largest range in Q^2 available for any excited baryon resonance. These results are shown in Fig. 6. Both quark-based approaches show excellent agreement with the data at $Q^2 > 1$–2 GeV^2 and confirm the presence of a strong quark core as probed in electroproduction at the shorter distance scales. The attempt to describe the transition amplitude solely within a dynamically generated resonance models (DGR), underestimates the resonance strength even at the lowest Q^2 where dynamical processes may make significant contributions, and drops much more rapidly with Q^2 than the data, as expected for meson–baryon resonance contributions with a minimum of five quarks involved in the interaction compared to the minimum of the three quarks at the core of the quark model.

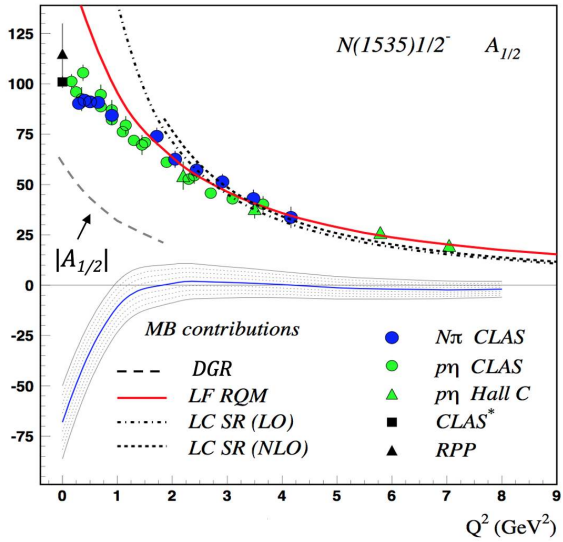

Fig. 6. Transition amplitude $A_{1/2}$ of $N(1535)1/2^-$. The theory curves are from the LF RQM [52] (solid red line), and the light-cone sum rule (dotted lines) [60] (LC SR) QCD approach. The dashed lines represent a dynamically generated resonance model [57].

Such data-based observations have contributed to today's prevailing view that the Roper resonance as well as $N^\star$ and $\Delta^\star$ resonances in the mass range below $W \sim 1.8$ GeV, all contain a three-quark core that defines the characteristics of the resonance at all length scales, and meson–baryon components involving five or more quarks. The latter component occupies distances close to the periphery of the excited state, while the former provides the quark core at distances close to the center.

4.2. Structure of the Roper resonance from lattice QCD

The structure of the $N(1440)1/2^+$ resonance, as represented by the transition form factors F_1 and F_2, has also been investigated in lattice QCD simulations, albeit at relatively large pion masses from 390 to 875 MeV [61]. The results are shown in Fig. 7. In kinematics where the simulation overlaps with the data, for the lowest pion mass, one sees an agreement of the lattice calculations with the experimental results.

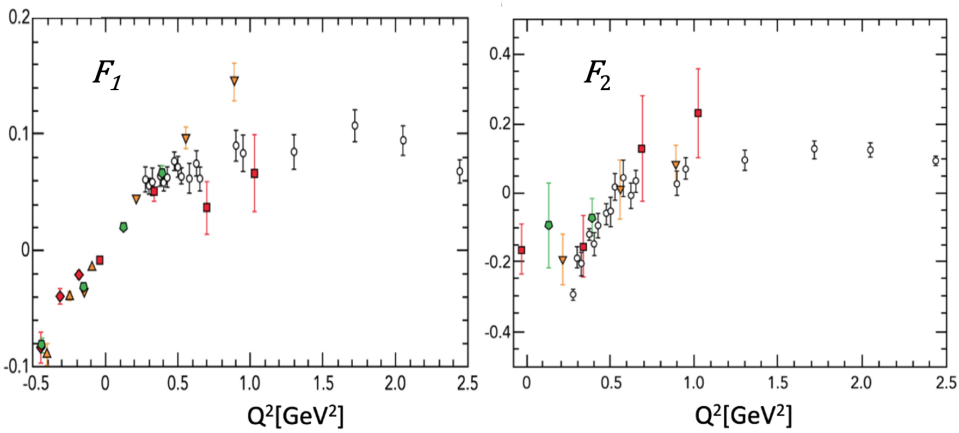

Fig. 7. Roper resonance transition form factor. Left: $F_1(t)$, right: $F_2(t)$. The open circles are the CLAS data. The other (colored) symbols represent LQCD data. Lattice results are for pion masses 390 MeV (red squares), 450 MeV (orange triangles), and 875 MeV (green pentagons).

5. Higher-mass scalar excitations of the nucleon

In quark models, baryons are described as systems of three constituent quarks, each with spin 1/2. The total baryonic wave function must be antisymmetric with respect to the exchange of any two quarks. The color wave function is completely antisymmetric (A), while the combined space–spin–flavor wave function is symmetric (S).

If the three quarks have identical masses, their spin–flavor wave functions obey SU(6) symmetry. The flavor wave functions of the nucleon and its excitations are characterized by isospin $I = 1/2$ and exhibit mixed symmetry (τ_{M_S,M_A}). The spin wave function χ can also have mixed symmetry (χ_{M_S,M_A} for spin $S = 1/2$) or be symmetric (χ_S for $S = 3/2$).

The spin–flavor wave functions can therefore assume the configurations ^{2}8[56], ^{2}8[70], ^{4}8[70], and ^{2}8[20], where the [56]-plet is fully symmetric, the [70]-plets have mixed symmetry, and the [20]-plet is fully antisymmetric.

The spatial dynamics of the three quarks are described by the time-dependent Jacobi coordinates $\vec{\rho} = \frac{1}{\sqrt{2}}(\vec{r}_1 - \vec{r}_2)$, $\vec{\lambda} = \frac{1}{\sqrt{6}}(\vec{r}_1 + \vec{r}_2 - 2\vec{r}_3)$, and the trivial center-of-mass coordinate. In the harmonic-oscillator (h.o.) approximation, both oscillators can be excited with orbital angular momenta l_ρ and l_λ, and can also undergo radial excitations n_ρ and n_λ. Thus, the h.o. wave functions are characterized as $\phi_{l_\rho n_\rho; l_\lambda n_\lambda}$.

Resonances with $l_\rho + 2n_\rho + l_\lambda + 2n_\lambda = N$ belong to the N^{th} excitation shell. The symmetry of the spatial wave function ϕ must ensure the overall symmetry of the combined space–spin–flavor wave function.

In the second excitation shell, four resonances with quantum numbers $I(J^P) = 1/2(1/2^+)$ are expected. The symmetry of their space–spin–flavor wave functions is given by

$$
\begin{aligned}
&^2\text{8}[56]: \quad (\phi_S\,\chi_{M_S}\,\tau_{M_S} + \phi_S\,\chi_{M_A}\,\tau_{M_A})\,;\\
&^2\text{8}[70]: \quad (\phi_{M_A}\,\chi_{M_A}\,\tau_{M_S} - \phi_{M_S}\,\chi_{M_S}\,\tau_{M_S} + \phi_{M_S}\,\chi_{M_A}\,\tau_{M_A} - \phi_{M_A}\,\chi_{M_S}\,\tau_{M_A})\,;\\
&^4\text{8}[70]: \quad (\phi_{M_S}\,\chi_S\,\tau_{M_S} + \phi_{M_A}\,\chi_S\,\tau_{M_A})\,;\\
&^2\text{8}[20]: \quad (\phi_A\,\chi_{M_A}\,\tau_{M_S} + \phi_A\,\chi_{M_S}\,\tau_{M_A})\,.
\end{aligned}
$$

The spatial wave function of N^*s in the second excitation shell can be cast into the form

$$
\begin{aligned}
&^2\text{8}[56]: \quad \phi_S(l_\rho n_\rho; l_\lambda n_\lambda) &&= (\phi_{0100} + \phi_{0001})/\sqrt{2}\,;\\
&^2\text{8}[70]: \quad \phi_{M_S}(l_\rho n_\rho; l_\lambda n_\lambda) &&= (\phi_{0100} - \phi_{0001})/\sqrt{2}\,; \quad \phi_{M_A}(l_\rho n_\rho; l_\lambda n_\lambda) = \phi_{1010}\,;\\
&^4\text{8}[70]: \quad \phi_{M_S}(l_\rho n_\rho; l_\lambda n_\lambda) &&= (\phi_{2000} - \phi_{0020}/\sqrt{2})\,; \quad \phi_{M_A}(l_\rho n_\rho; l_\lambda n_\lambda) = \phi_{1010}\,;\\
&^2\text{8}[20]: \quad \phi_A(l_\rho n_\rho; l_\lambda n_\lambda) &&= \phi_{1010}\,. \qquad (2)
\end{aligned}
$$

These are harmonic-oscillator (h.o.) wave functions. The true wave functions, however, are mixtures of these basis states. In principle, the nucleon and states from the fourth excitation shell could also contribute to the wave function of a given resonance, but mixing between different shells is expected to be small and is therefore neglected.

The mixing parameters for the non-relativistic quark model of Isgur and Karl [29] and for the relativistic Bonn model [32] are listed in Table 3, together with the corresponding masses. Both models contain free parameters

that are adjusted to reproduce the observed Breit–Wigner masses; hence, their predictions should be compared to the experimental Breit–Wigner values.

Table 3. Masses and configuration mixing for the excited states of the nucleon with $J^P = 1/2^+$ in the second excitation shell from [29] ([32]). The masses are in MeV, the contributions in %.

	$M_{\rm RPP}$	$M_{\rm calc}$	^{2}8[56]	^{2}8[70]	^{4}8[70]	^{2}8[20]
$N(1440)$	1440±30	1405 (1518)	97.0 (90.8)	3.0 (6.1)	0 (0.1)	0 (0.2)
$N(1710)$	1710±30	1705 (1729)	2.6 (15.5)	87.4 (81.4)	9.5 (0.7)	0.5 (0.3)
$N(1880)$	1880±50	1890 (1950)	0.4 (0.9)	9.0 (0.9)	70.3 (88.6)	20.3 (7.4)
$N(2100)$	2100±50	2055 (1996)	0.0 (34.2)	0.6 (5.9)	20.2 (6.8)	79.2 (50.8)

Four states with quantum numbers $I(J^P) = 1/2(1/2^+)$ are predicted, and indeed four such resonances are observed experimentally: $N(1440)1/2^+$, $N(1710)1/2^+$, $N(1880)1/2^+$, and $N(2100)1/2^+$. It is therefore tempting to identify these experimentally established resonances with the corresponding quark-model states.

Both models agree that the Roper resonance is predominantly the first radial excitation of the nucleon, with only small admixtures from higher configurations. Of course, the Roper may also possess a meson cloud, which is not accounted for in simple quark models. Nevertheless, its structure is largely governed by its three-quark core. This observation lends support to interpreting $N(1710)1/2^+$ as the second radial excitation [38]. However, this conjecture is not supported by electroproduction data.

Figure 8 compares the $N(1440)1/2^+$ and $N(1710)1/2^+$ transition form factors. The Roper transition form factor crosses zero due to the node in its wave function, with the position of the zero shifted by meson-cloud effects. For a second radial excitation, two zero crossings could be expected, but such behavior is not observed experimentally. In quark models, both $N(1440)1/2^+$ and $N(1710)1/2^+$ possess one node: the $N(1440)1/2^+$ in $\rho^2+\lambda^2$, and the $N(1710)1/2^+$ in $\rho^2-\lambda^2$ (see the inset in Fig. 8). The node in $\rho^2-\lambda^2$ does not result in a zero crossing of the transition amplitude.

The transition form factor for $N(1880)1/2^+$ is not yet known, but it appears plausible to assign this state to the expected member of a spin quartet with $L = 2$ and $S = 3/2$, coupling to $J = 1/2$. This quartet should be accompanied by three additional states with $L = 2$, $S = 3/2$, coupling to $J = 3/2$, $5/2$, and $7/2$. These may correspond to the experimentally observed resonances $N(1900)3/2^+$, $N(1860)5/2^+$, and $N(1990)7/2^+$.

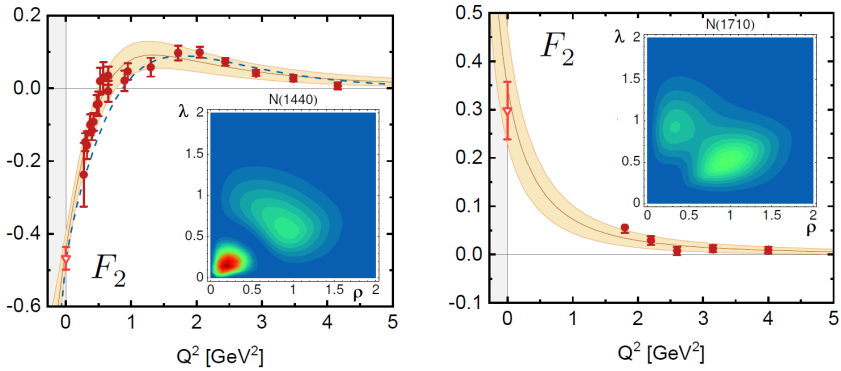

Fig. 8. Transition form factor $F_2(Q^2)$ for the $N(1440)1/2^+$ and $N(1710)1/2^+$. The data are from Refs. [55, 62], the band is from [63] and the dashed curve from [64]. The quark-model spatial probability distributions from [65] are shown as insets.

The $N(2100)1/2^+$ resonance remains a puzzle. In a first interpretation, it could be assigned a dominant ^{2}[20] configuration. In the leading spatial component of this configuration, both oscillators are excited, see ϕ_A in Eq. (2). In Ref. [29], this contribution amounts to approximately 80%, implying that production in a single-step process should be strongly suppressed. In contrast, Ref. [32] finds a suppression by only about a factor of two.

Alternatively, $N(2100)1/2^+$ could be interpreted as a hybrid baryon. Mesonic hybrids with an excited gluon field, often denoted as $q\bar{q}g$ mesons, were predicted [66] soon after QCD was established as the theory of the strong interaction (see Ref. [67] for a review). Mesonic hybrids may possess *exotic* quantum numbers — combinations that are not accessible to conventional $q\bar{q}$ systems. They are predicted to decay primarily through string breaking, leading to two-meson final states in which one of the mesons carries intrinsic orbital angular momentum [68, 69]. This selection rule is broken when the quark and antiquark masses are unequal. A candidate for such a state, the $\pi_1(1600)$ with $J^{PC} = 1^{-+}$, has been identified unambiguously in its decays to $f_1(1285)\pi$ [70], $b_1(1235)\pi$ [71, 72], $\eta'\pi$ [70], $\rho\pi$ [73], and $\eta\pi$ [74]; see Ref. [75] for a review.

Hybrid baryons, in contrast, do not possess exotic quantum numbers. Their identification must therefore rely on comparisons with mass predictions and decay patterns. Lattice QCD calculations have predicted the masses of hybrid baryons [43, 76]. Figure 9 shows the expected mass spectra of N^* states with $J^P = 1/2^+$ and $3/2^+$ and of Δ^* states with $J^P = 5/2^+$ and $7/2^+$. These calculations were performed with quark masses corresponding to a pion mass of about 400 MeV; hence, all predicted masses are systematically too high. In Fig. 9, all masses are normalized to the nucleon mass. The $\Delta(1950)7/2^+$ appears near 1900 MeV, lending support to the calculations.

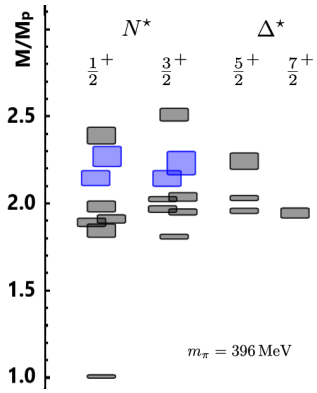

Fig. 9. Mass spectra of N^* and Δ^* baryons. The mass scale is made to reproduce the masses of the nucleon and of $\Delta(1950)7/2^+$. Baryons with a large hybrid content are highlighted in blue. Adapted from [43].

The four $I(J^P) = 1/2(1/2^+)$ states discussed here are all observed below 2 GeV. Above this region, a mass gap is seen: the next qqq state, belonging to the fourth excitation shell, is expected at about 2.4 GeV. Within this gap (2.0–2.4 GeV), two hybrid baryons are predicted. Thus, if the $N(2100)1/2^+$ is not a member of the [20]-plet, it could plausibly be interpreted as a hybrid baryon. By analogy with hybrid mesons, one expects hybrid baryons to decay predominantly into a baryon–meson pair in which one of the final-state hadrons carries one unit of intrinsic orbital angular momentum.

A third possibility remains: $N(2100)1/2^+$ could represent the lowest-mass $J^P = 1/2^+$ state in the fourth excitation shell, its mass lowered analogously to the Roper resonance in the second shell. In this interpretation, it would belong to a $^2 8[56]$ configuration, and its wave function would be given by

$$\phi_{l_\rho n_\rho, l_\lambda, n_\lambda,} = \frac{1}{\sqrt{6}}\,\phi_{02,00} + \frac{1}{\sqrt{6}}\,\phi_{00,02} + \frac{\sqrt{5}}{3}\,\phi_{01,01} - \frac{1}{3}\,\phi_{20,20}\,. \qquad (3)$$

What do we expect? For a member of the [20]-plet with a spatial wave function $\phi_{l_\rho n_\rho, l_\lambda n_\lambda} = \phi_{10,10}$, we expect that a first de-excitation leads to spatial wave functions of the form $\phi_{10,00}$ or $\phi_{00,10}$, corresponding to one unit of orbital angular momentum. The two oscillators may also de-excite coherently through pion emission, where the two pions form a $f_0(500)$. Configuration mixing introduces components from $^2 8[56]$, $^2 8[70]$, and $^4 8[70]$, which can decay into $N\pi$, $N\rho$, or $\Delta(1232)\pi$ final states without intrinsic orbital angular momentum.

For a hybrid state, we expect decays into a baryon–meson pair where one of the hadrons carries intrinsic orbital angular momentum. Since the decay products have unequal masses, the symmetry that would otherwise

enforce the angular-momentum distribution is broken, allowing also S-wave decays into channels such as $N\pi$, $N\rho$, or $\Delta(1232)\pi$. Nevertheless, a substantial fraction of the decays should proceed through intermediate states such as $N(1535)1/2^-$, $N(1520)3/2^-$, or $Nf_0(500)$, where the latter represents correlated two-pion emission.

If $N(2100)1/2^+$ is instead a Roper-like state belonging to the fourth excitation shell, we expect contributions from components of the type $\phi_{l_\rho n_\rho, l_\lambda n_\lambda} = \phi_{20,20}$, corresponding to intrinsic orbital angular momentum $L = 2$ in one of the outgoing hadrons. The $\phi_{01,01}$ component could contribute to decays into radially excited states such as $N(1440)1/2^+$ or $N(1710)1/2^+$. The $\phi_{20,20}$ component is likely to decay into $N(1680)5/2^+, \pi$ in an F-wave, $N(1720)3/2^+, \pi$ in a P-wave, or $N, f_2(1270)$ in a D-wave. The latter two components can also emit two pions coherently from the two excited oscillators, leading to $Nf_0(500)$ as an intermediate state.

Table 4 presents preliminary results from a BnGa coupled-channel analysis that includes new data from the CBELSA/TAPS experiment [77], both with and without polarization observables. The decays listed in the first two rows may originate from the $\phi_{02,00}$ and $\phi_{00,02}$ components, while the $Nf_0(500)$ decays can be interpreted as correlated two-pion emission from the $\phi_{20,20}$ and $\phi_{01,01}$ configurations. The $N(1720)3/2^+, \pi$ and $N(1710)1/2^+$ decay modes are naturally expected for a Roper-like $J^P = 1/2^+$ resonance belonging to the fourth excitation shell.

Table 4. Branching ratios (in %) for decays of the $N(2100)1/2^+$ [77] (preliminary). The sum is (116±13)%.

$N\pi$	$N\eta$	$N\eta'$	
16±4	9±4	4±2	
ΛK	ΣK	$\Delta\pi$	$N\rho$
< 1	7±3	10±4	17±7
$N_{1535}\pi$	$N_{1710}\pi$	$N_{1720}\pi$	$Nf_0(500)$
< 1	10±5	15±5	28±6

These interpretations are clearly suggestive. There is no selection rule that would forbid the $\phi_{02,00}$ and $\phi_{00,02}$ components from decaying into orbitally or radially excited intermediate states, and the $\phi_{20,20}$ and $\phi_{01,01}$ components could decay, for instance, into $N(1720)3/2^+, \pi$, with subsequent rescattering of the $N(1720)1/2^+, \pi$ system into $N\rho$ or $\Delta(1232)\pi$. However, the most straightforward interpretation of the results is that $N(2100)1/2^+$ represents a low-mass member of the fourth excitation shell.

In summary, the sequence of positive-parity N^* resonances with $J^P = 1/2^+$ — from the Roper resonance $N(1440)1/2^+$ through $N(1710)1/2^+$, $N(1880)1/2^+$, and up to $N(2100)1/2^+$ — reveals a consistent pattern in the excitation spectrum of the nucleon. The Roper resonance is now well understood as the first radial excitation of the nucleon, dominated by its three-quark core and dressed by a substantial meson cloud. The higher states may naturally be interpreted as successive excitations within the same quark-model framework, with increasing contributions from orbital motion and configuration mixing. While alternative interpretations, such as dynamically generated or hybrid baryons, cannot be excluded, the most coherent picture emerging from both quark-model and coupled-channel analyses identifies $N(2100)1/2^+$ as a low-mass member of the fourth excitation shell — a Roper-like state completing the observed pattern of nucleon excitations.

The work of V. Burkert was supported by the U.S. Department of Energy under contract DE-AC-06OR23177.

REFERENCES

[1] L.D. Roper, «Evidence for a P_{11} Pion–Nucleon Resonance at 556 MeV», *Phys. Rev. Lett.* **12**, 340 (1964).

[2] H.L. Anderson, E. Fermi, E.A. Long, D.E. Nagle, «Total Cross-sections of Positive Pions in Hydrogen», *Phys. Rev.* **85**, 936 (1952).

[3] B.T. Feld, W.M. Layson, «Evidence for a possible π–N resonance in the $P_{1/2}, T = 1/2$ state», in: «11$^{\text{th}}$ International Conference on High-energy Physics», Geneva, Switzerland 4–11 July 1962, pp. 147–151, https://cds.cern.ch/record/2009199?ln=pl

[4] V.D. Burkert, C.D. Roberts, «*Colloquium*: Roper resonance: Toward a solution to the fifty year puzzle», *Rev. Mod. Phys.* **91**, 011003 (2019).

[5] S. Navas *et al.*, «Review of Particle Physics», *Phys. Rev. D* **110**, 030001 (2024).

[6] G. Höhler, F. Kaiser, R. Koch, E. Pietarinen, «Physics Data: Handbook of pion–nucleon scattering», *Phys. Daten* **12N1**, 1 (1979).

[7] R.E. Cutkosky *et al.*, «Pion–Nucleon Partial Wave Analysis», in: «4$^{\text{th}}$ International Conference on Baryon Resonances», Toronto, Canada July 14–16, 1980.

[8] M. Batinić, S. Ceci, A. Švarc, B. Zauner, «Poles of the Zagreb analysis partial-wave T matrices», *Phys. Rev. C* **82**, 038203 (2010).

[9] M. Shrestha, D.M. Manley, «Multichannel parametrization of πN scattering amplitudes and extraction of resonance parameters», *Phys. Rev. C* **86**, 055203 (2012).

[10] CBELSA/TABS Collaboration (V. Sokhoyan *et al.*), «High-statistics study of the reaction $\gamma p \to p\, 2\pi^0$», *Eur. Phys. J. A* **51**, 95 (2015); *Erratum ibid.* **51**, 187 (2015).

[11] B.C. Hunt, D.M. Manley, «Updated determination of N^* resonance parameters using a unitary, multichannel formalism», *Phys. Rev. C* **99**, 055205 (2019).

[12] A.V. Sarantsev *et al.*, «Decays of N^* and Δ^* resonances into $N\rho$, $\Delta\pi$, and $Nf_0(500)$», *Phys. Rev. C* **112**, 015202 (2025).

[13] G. Penner, U. Mosel, «Vector meson production and nucleon resonance analysis in a coupled-channel approach for energies $m_N < \sqrt{s} < 2$ GeV. I. Pion-induced results and hadronic parameters», *Phys. Rev. C* **66**, 055211 (2002).

[14] R.A. Arndt, W.J. Briscoe, I.I. Strakovsky, R.L. Workman, «Extended partial-wave analysis of πN scattering data», *Phys. Rev. C* **74**, 045205 (2006).

[15] T.P. Vrana, S.A. Dytman, T.S.H. Lee, «Baryon resonance extraction from πN data using a unitary multichannel model», *Phys. Rep.* **328**, 181 (2000).

[16] V. Shklyar, H. Lenske, U. Mosel, «η-meson production in the resonance-energy region», *Phys. Rev. C* **87**, 015201 (2013).

[17] G. Höhler, «Determination of πN resonance pole parameters», *PiN Newslett.* **1993**, 1 (1993).

[18] V. Burkert *et al.*, «Note on the definitions of branching ratios of overlapping resonances», *Phys. Lett. B* **844**, 138070 (2023).

[19] M. Hoferichter, J.R. de Elvira, B. Kubis, U.-G. Meißner, «Nucleon resonance parameters from Roy–Steiner equations», *Phys. Lett. B* **853**, 138698 (2024).

[20] D. Rönchen, M. Döring, U.-G. Meißner, C.-W. Shen, «Light baryon resonances from a coupled-channel study including $K\Sigma$ photoproduction», *Eur. Phys. J. A* **58**, 229 (2022).

[21] A.V. Anisovich *et al.*, «Neutron helicity amplitudes», *Phys. Rev. C* **96**, 055202 (2017).

[22] D. Rönchen *et al.*, «Eta photoproduction in a combined analysis of pion- and photon-induced reactions», *Eur. Phys. J. A* **51**, 70 (2015).

[23] A. Švarc *et al.*, «Poles of Karlsruhe–Helsinki KH80 and KA84 solutions extracted by using the Laurent–Pietarinen method», *Phys. Rev. C* **89**, 045205 (2014).

[24] W. Chen *et al.*, «Amplitude analysis of $\gamma n \to \pi^- p$ data above 1 GeV», *Phys. Rev. C* **86**, 015206 (2012).

[25] E.N. Argyres, R. Atkinson, «Self-Consistency and the Roper Resonance», *Phys. Rev.* **159**, 1446 (1967).

[26] P. Chýlek, «Roper Resonance $N(1470)$ in the Three-Quark Model», *Prog. Theor. Phys.* **40**, 1453 (1968).

[27] J.-M. Richard, «Level order of quark systems: The puzzle of the Roper resonance, and related questions», *Acta Phys. Pol. B* **57**, 2-A12 (2026), this issue, arXiv:2506.07764 [hep-ph].

[28] N. Isgur, G. Karl, «P-wave baryons in the quark model», *Phys. Rev. D* **18**, 4187 (1978).

[29] N. Isgur, G. Karl, «Positive-parity excited baryons in a quark model with hyperfine interactions», *Phys. Rev. D* **19**, 2653 (1979); *Erratum ibid.* **23**, 817 (1981).

[30] S. Capstick, N. Isgur, «Baryons in a relativized quark model with chromodynamics», *Phys. Rev. D* **34**, 2809 (1986).

[31] L.Y. Glozman, W. Plessas, K. Varga, R.F. Wagenbrunn, «Unified description of light- and strange-baryon spectra», *Phys. Rev. D* **58**, 094030 (1998).

[32] U. Löring, B.C. Metsch, H.R. Petry, «The light-baryon spectrum in a relativistic quark model with instanton-induced quark forces: The nonstrange baryon spectrum and ground states», *Eur. Phys. J. A* **10**, 395 (2001).

[33] M. Ronniger, B.C. Metsch, «Effects of a spin-flavour-dependent interaction on light-flavoured baryon helicity amplitudes», *Eur. Phys. J. A* **49**, 8 (2013).

[34] M.M. Giannini, E. Santopinto, A. Vassallo, «Hypercentral constituent quark model and isospin dependence», *Eur. Phys. J. A* **12**, 447 (2001).

[35] E. Santopinto, «An interacting quark–diquark model of baryons», *Phys. Rev. C* **72**, 022201 (2005).

[36] E. Santopinto, J. Ferretti, «Strange and nonstrange baryon spectra in the relativistic interacting quark–diquark model with a Gürsey and Radicati-inspired exchange interaction», *Phys. Rev. C* **92**, 025202 (2015).

[37] R. Bijker, F. Iachello, A. Leviatan, «Algebraic Models of Hadron Structure. I. Nonstrange Baryons», *Ann. Phys.* **236**, 69 (1994).

[38] S.J. Brodsky, G.F. de Téramond, H.G. Dosch, J. Erlich, «Light-front holographic QCD and emerging confinement», *Phys. Rep.* **584**, 1 (2015).

[39] V. Burkert, G. Eichmann, E. Klempt, «The impact of γN and $\gamma^* N$ interactions on our understanding of nucleon excitations», *Prog. Part. Nucl. Phys.* **146**, 104214 (2026), arXiv:2506.16482 [hep-ph].

[40] G. Eichmann, C.S. Fischer, H. Sanchis-Alepuz, «Light baryons and their excitations», *Phys. Rev. D* **94**, 094033 (2016).

[41] U.B. Kaulfuss, U.-G. Meißner, «The breathing mode of the modified skyrmion», *Phys. Lett. B* **154**, 193 (1985).

[42] Z.-p. Li, V. Burkert, Z.-j. Li, «Electroproduction of the Roper resonance as a hybrid state», *Phys. Rev. D* **46**, 70 (1992).

[43] J.J. Dudek, R.G. Edwards, «Hybrid baryons in QCD», *Phys. Rev. D* **85**, 054016 (2012).

[44] O. Krehl, C. Hanhart, S. Krewald, J. Speth, «What is the structure of the Roper resonance?», *Phys. Rev. C* **62**, 025207 (2000).

[45] D. Rönchen *et al.*, «Coupled-channel dynamics in the reactions $\pi N \to \pi N, \eta N, K\Lambda, K\Sigma$», *Eur. Phys. J. A* **49**, 44 (2013).

[46] D. Rönchen *et al.*, «Photocouplings at the pole from pion photoproduction», *Eur. Phys. J. A* **50**, 101 (2014); *Erratum ibid.* **51**, 63 (2015).

[47] S. Owa, D.B. Leinweber, A.W. Thomas, «Nucleon resonance structure to 2 GeV and the nature of the Roper», arXiv:2503.09945 [hep-ph].

[48] L. Hockley, C. Abell, D. Leinweber, A. Thomas, «Understanding the nature of the $\Delta(1600)$ resonance», *Phys. Rev. D* **111**, 076027 (2025), arXiv:2406.00981 [hep-ph].

[49] CLAS Collaboration (I.G. Aznauryan *et al.*), «Electroexcitation of nucleon resonances from CLAS data on single pion electroproduction», *Phys. Rev. C* **80**, 055203 (2009).

[50] I.G. Aznauryan, V.D. Burkert, «Electroexcitation of nucleon resonances», *Prog. Part. Nucl. Phys.* **67**, 1 (2012).

[51] A.J.F. Siegert, «Note on the Interaction Between Nuclei and Electromagnetic Radiation», *Phys. Rev.* **52**, 787 (1937).

[52] I.G. Aznauryan, V.D. Burkert, «Nucleon electromagnetic form factors and electroexcitation of low-lying nucleon resonances in a light-front relativistic quark model», *Phys. Rev. C* **85**, 055202 (2012).

[53] J. Segovia *et al.*, «Completing the Picture of the Roper Resonance», *Phys. Rev. Lett.* **115**, 171801 (2015).

[54] V.I. Mokeev *et al.*, «First results on nucleon resonance electroexcitation amplitudes from $ep \to e'\pi^+\pi^- p'$ cross sections at $W = 1.4$–1.7 GeV and $Q^2 = 2.0$–5.0 GeV^2», *Phys. Rev. C* **108**, 025204 (2023).

[55] CLAS Collaboration (V.I. Mokeev *et al.*), «Experimental Study of the $P_{11}(1440)$ and $D_{13}(1520)$ resonances from CLAS data on $ep \to e'\pi^+\pi^- p'$», *Phys. Rev. C* **86**, 035203 (2012).

[56] A1 Collaboration (S. Štajner *et al.*), «Beam-Recoil Polarization Measurement of π^0 Electroproduction on the Proton in the Region of the Roper Resonance», *Phys. Rev. Lett.* **119**, 022001 (2017).

[57] D. Jido, M. Döring, E. Oset, «Transition form factors of the $N^*(1535)$ as a dynamically generated resonance», *Phys. Rev. C* **77**, 065207 (2008).

[58] P.C. Bruns, M. Mai, U.-G. Meißner, «Chiral dynamics of the $S_{11}(1535)$ and $S_{11}(1650)$ resonances revisited», *Phys. Lett. B* **697**, 254 (2011).

[59] N. Kaiser, P.B. Siegel, W. Weise, «Chiral dynamics and the $S_{11}(1535)$ nucleon resonance», *Phys. Lett. B* **362**, 23 (1995).

[60] I.V. Anikin, V.M. Braun, N. Offen, «Electroproduction of the $N^*(1535)$ nucleon resonance in QCD», *Phys. Rev. D* **92**, 014018 (2015).

[61] H.-W. Lin, S.D. Cohen, «Roper properties on the lattice: An update», *AIP Conf. Proc.* **1432**, 305 (2012).

[62] CLAS Collaboration (K. Park *et al.*), «Measurements of $ep \to e'\pi^+ n$ at $1.6 < W < 2.0$ GeV and extraction of nucleon resonance electrocouplings at CLAS», *Phys. Rev. C* **91**, 045203 (2015).

[63] G. Eichmann, G. Ramalho, «Nucleon resonances in Compton scattering», *Phys. Rev. D* **98**, 093007 (2018).

[64] D. Drechsel, S.S. Kamalov, L. Tiator, «Unitary isobar model — MAID2007», *Eur. Phys. J. A* **34**, 69 (2007).

[65] T. Melde, W. Plessas, B. Sengl, «Quark-model identification of baryon ground and resonant states», *Phys. Rev. D* **77**, 114002 (2008).

[66] D. Horn, J. Mandula, «A model of mesons with constituent gluons», *Phys. Rev. D* **17**, 898 (1978).

[67] F. Gross *et al.*, «50 Years of quantum chromodynamics», *Eur. Phys. J. C* **83**, 1125 (2023).

[68] N. Isgur, R. Kokoski, J. Paton, «Gluonic excitations of mesons: Why they are missing and where to find them», *Phys. Rev. Lett.* **54**, 869 (1985).

[69] R. Kokoski, N. Isgur, «Meson decays by flux-tube breaking», *Phys. Rev. D* **35**, 907 (1987).

[70] E852 Collaboration (J. Kuhn *et al.*), «Exotic meson production in the $f_1(1285)\pi^-$ system observed in the reaction $\pi^- p \to \eta\pi^+\pi^-\pi^- p$ at 18 GeV/c», *Phys. Lett. B* **595**, 109 (2004).

[71] E852 Collaboration (M. Lu *et al.*), «Exotic Meson Decay to $\omega\pi^0\pi^-$», *Phys. Rev. Lett.* **94**, 032002 (2005).

[72] C.A. Baker *et al.*, «Confirmation of $a_0(1450)$ and $\pi_1(1600)$ in $\bar{p}p \to \omega\pi^+\pi^-\pi^0$ at rest», *Phys. Lett. B* **563**, 140 (2003).

[73] M. Aghasyan *et al.*, «Light isovector resonances in $\pi^- p \to \pi^-\pi^-\pi^+ p$ at 190 GeV/c», *Phys. Rev. D* **98**, 092003 (2018).

[74] B. Kopf *et al.*, «Investigation of the lightest hybrid meson candidate with a coupled-channel analysis of $\bar{p}p$-, $\pi^- p$- and $\pi\pi$-Data», *Eur. Phys. J. C* **81**, 1056 (2021).

[75] B. Grube, «Exotic mesons», Chapter 8.3 in: *Eur. Phys. J. C* **83**, 1125 (2023).

[76] T. Khan, D. Richards, F. Winter, «Positive-parity baryon spectrum and the role of hybrid baryons», *Phys. Rev. D* **104**, 034503 (2021).

[77] A. Sarantsev *et al.*, «Decays of scalar excitations of the nucleon from new data on $\gamma p \to p\pi^0\pi^0$», 2025, in preparation.